PAPER

Check for updates

Enhancing the performance of Ni nanoparticle modified carbon felt towards glycerol electrooxidation: impact of organic additive

Mohamed E. Ghaith, [ID] Muhammad G. Abd El-Moghny, [ID] * Hafsa H. Alalawy, Mohamed E. El-Shakre and Mohamed S. El-Deab [ID] *

Organic additives are widely used in the deposition baths of metals and alloys thanks to their special function which affects the growth and the building of the crystal. This study investigates the effect of glycerol on Ni deposition onto carbon felt (CF) and its effect on the catalytic activity towards glycerol electrooxidation. The impact of glycerol on the morphology, distribution, and particle size of the electrodeposited Ni is disclosed using a scanning electron microscope (SEM). X-ray diffraction (XRD), X-ray photoelectron spectroscopy (XPS), and cyclic voltammetry (CV) techniques were used to probe the possible changes of the electrodeposited Ni oxide phases. Electrochemical measurements show that the as-synthesized $Ni_{0.05}$@CF electrocatalyst prepared in the presence of 50 mM glycerol has a marked activity towards glycerol electrooxidation, as confirmed by the impressive increase of the oxidation current by about 1.6 times concurrently with a favorable negative shift of its onset potential. Moreover, the charge transfer resistance (R_{ct}) is much reduced from 140 to 87 ohm. The addition of glycerol to the deposition bath is believed to retard the growth of the formed Ni deposits while enhancing the nucleation rate and thus increases the particle density and, consequently, the distribution of deposited Ni over the entire CF is improved along with increasing the surface concentration and surface-active sites. This assumption is supported by density functional theory (DFT) calculations.

1. Introduction

Direct alcohol fuel cells (DAFCs) are one of the recent technologies suggested for supplying sustainable energy because of the abundance of feeding fuels.[1] The most common fuel used is methanol owing to its relatively cheap cost, being consistently available, and having high energy density (4820 W h L^{-1}), good electrical activity, and biodegradability. However, it is toxic with poor stability and high volatility in addition to a crossover problem. Other fuels have been used, *e.g.* ethanol, due to its being nontoxic with high-energy density (6280 W h L^{-1}), although it is difficult to undergo complete oxidation to CO_2 at low temperatures due to its strong C–C bond. Considering this, glycerol seems to be promising to use as a fuel in DAFC in view of its nontoxicity, and cheap cost because it is considered a by-product of many processes especially biodiesel production, low flammability, low volatility, low crossover, and high energy density (6400 W h L^{-1}).[2,3] Additionally, the complete oxidation of glycerol generates 14 electrons producing many oxidized products. The overproduction of glycerol per year secures it as an alternative fuel of low cost. Moreover, the presence of the three hydroxyl groups in glycerol allows to produce of more valuable products in many ways and electrooxidation production

is found to be the easiest way from which many valuable products can be obtained such as glyceraldehyde and dihydroxyacetone, glyceric acid, mesoxalic acid, tartronic acid, and glycolic acid. Remarkably, glycerol can be used to assist the anodic reaction in the water electrolysis process which is thermodynamically more favored than the oxygen evolution reaction to save the input energy.[3–7]
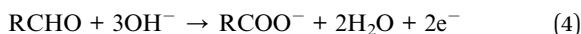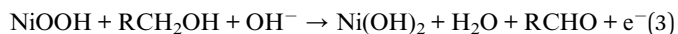
Nickel-based catalysts have been reported previously as excellent catalysts for several applications, especially in electrocatalysis such as water splitting,[8–15] fuel cells,[16–19] oxidation of many organic molecules (methanol, ethanol, glucose, urea, and glycerol).[20–37] This is attributed to its high stability in alkaline medium, low cost, high electro-catalytic activity, good electrical conductivity, and ease of active phase formation. Moreover, nickel-based electrocatalysts can be used as cheap and efficient electrocatalysts for DAFCs and become a substitute for expensive noble metals.[28]

The mechanism of the glycerol electrooxidation over the Ni catalyst according to Fleischmann *et al.* mechanism is illustrated in eqn (1)–(4):[38]

$$Ni + 2OH \rightarrow Ni(OH)_2 + 2e^- \quad (1)$$

$$Ni(OH)_2 + OH^- \rightarrow NiOOH + H_2O + e^- \quad (2)$$
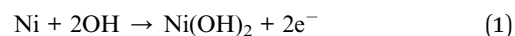
Chemistry Department, Faculty of Science, Cairo University, Egypt. E-mail: mugamal@cu.edu.eg; msaada@sci.cu.edu.eg

$$NiOOH + RCH_2OH + OH^- \rightarrow Ni(OH)_2 + H_2O + RCHO + e^- \quad (3)$$

$$RCHO + 3OH^- \rightarrow RCOO^- + 2H_2O + 2e^- \quad (4)$$

From the previously mentioned mechanism, the active component in the Ni-based catalysts can be considered to be NiOOH.[38]

Various strategies are used to improve the catalytic activity of Ni electrocatalyst toward glycerol electro-oxidation. For instance, the addition of another metal such as Co, Cu, Fe, Bi, and Cr.[39–42] Habibi et al.[43] reported enhanced electrocatalytic activity of Ni by about 1.6 and 1.2 times via simple alloying of Ni with Co or Cu, respectively. El Nagar et al. observed that the insertion of Ni into Cu dendrites significantly enhances the activity and stability of the catalyst.[44] Moreover, modification of the surface of the catalyst or substrate improves the morphology and distribution of Ni. Ghaith et al.[45] showed that the catalytic activity of Ni was enhanced by 2.5 times via electrochemical treatment of the substrate in 1 M sulfuric acid. Houache et al.[34] improved the catalytic performance of the Ni by 9 times after surface treatment of the catalyst by using a sinusoidal wave. Another way to improve the catalytic activity of Ni-based electrocatalysts could be achieved via controlling the rate of nucleation and growth of Ni during its electrodeposition. This can be verified by adjusting the electrodeposition bath chemistry by adding, e.g., organic molecules containing O, N, and/or S which form free radical adsorbed on the electrodeposited metal and at the same time adsorbed on the substrate thus addition of the organic molecules retards the rate of growth and enhances the nucleation rate consequently forming smaller particle size with the homogeneous distribution.[46–48]

Catalyst' supporting materials play a vital role in determining the performance of the catalyst where the main parameters affecting the efficiency of the supporting material are surface area, surface functional groups, porosity, electrical conductivity, and electrochemical stability.[49–51] Carbon-based materials such as reticulated vitreous carbon (RVC), carbon sponge (CS), carbon felt (CF) or carbon paper (CP) are suitable candidates thanks to their high surface area, excellent porosity, chemical inertness, mechanical stability, good conductivity and favorable interaction between catalyst and its support. Compared to CF, these materials show some drawbacks as the high cost of preparation of RVC and rigid properties of CP (non-woven) due to the presence of the binder such as polytetrafluoroethylene.[52] Therefore, CF is the most suitable candidate. On the other hand, CF suffers from some disadvantages such as low wettability (high hydrophobic nature) which prevent the uniform distribution of the catalyst, but this drawback can be overcome via surface treatment methods such as electrochemical and thermal techniques.[53–59]

Herein, a simple procedure is introduced to control the agglomeration of the (Ni nanoparticles) during its electrodeposition onto CF without any prior surface treatment by using glycerol as an additive. The growth and the building of the crystal are much affected as well as the Ni surface active sites depending on the concentration of glycerol in the deposition bath of Ni particle size of the catalyst, then the activity is investigated towards glycerol electrooxidation in an alkaline medium, and finally Density functional theory (DFT) calculation is used to rationalize the obtained results.

2. Experimental

2.1. Materials

All the used chemicals are of analytical grade and are used as received without any further purification. All the solutions are prepared using distilled water. Sodium hydroxide (NaOH), nickel sulfate hexahydrate ($NiSO_4 \cdot 6H_2O$, 99.999%), sulfuric acid (99.95%) are purchased from Sigma-Aldrich, and carbon felt (CF, SGL, GFA 4 EA).

2.2. Electrode's preparation

Commercial CF sheets are cut (4 mm nominal thickness, 2 mm width, and 3 mm length) connected with a GC rod with 1 mm diameter and are used as a substrate for further modification with Ni nanoparticles.

The CF pieces are modified with Ni nanoparticles (Ni@CF) electrodeposited by employing the chronocoulometric technique from 0.1 M Na_2SO_4 containing 4 mM $NiSO_4$ at −1.0 V vs. SCE. The metal loading for all the prepared electrodes is 30 µg. The electrodeposition in the presence of various glycerol concentrations (0.025, 0.05, 0.5, 0.75, 0.1, 0.2, 0.3, 0.4, and 0.5 M) is studied given a symbol Ni_x@CF where x is the concentration of glycerol added to the bath. After the electrodeposition of Ni on the CF, the obtained electrode is washed with distilled water to remove all the glycerol on the working electrode. The obtained metallic Ni is activated by cycling the potential in 0.1 M NaOH solution between 0.0 and 0.7 V vs. SCE at a potential scan rate of 200 mV s^{-1} for 40 cycles then the characteristic peaks were obtained by scanning the potential at 10 mV s^{-1} rate in the same solution. The mass of the electrodeposited Ni is estimated from the amount of passed charge during the electrodeposition using Faraday's law of electrolysis. As no significant hydrogen evolution development is observed, thus the deposition efficiency is considered as 100%.[60]

2.3. Electrochemical and material characterizations

2.3.1. Electrochemical measurements. BioLogic potentiostat (model VSP-300) is used to perform all the electrochemical measurements at room temperature (25 ± 1 °C). Three electrodes setup are used in which Ni_x@CF, graphite rod, and saturated calomel electrode (SCE) act as working, counter, and reference electrodes, respectively. Cyclic voltammetry (CV), linear sweep voltammetry (LSV), chronoamperometry (CA), chronocoulometric technique, and electrochemical impedance spectroscopy (EIS) techniques are used to investigate the performance of the prepared catalysts towards electrooxidation of glycerol in 0.1 M NaOH aqueous solution containing 8 mM glycerol.

2.3.2. Material characterization. The crystallographic orientation, morphology, and chemical composition of the as-prepared catalysts are investigated by X-ray diffraction technique (XRD, Cu Kα radiation, STOE STADI) and field emission scanning electron microscope (FE-SEM, QUANTA FEG 250)

coupled with an energy dispersive X-ray spectrometer (EDX) unit, respectively. X-ray photoelectron spectroscopy (XPS), with a CLAM4 electron analyzer from Thermo VG Scientific, and an Mg Kα X-ray source (1253.6 eV) XR 50 from SPECS is used to determine the states of elements on the surface of the various samples.

2.3.3. Computational methods. The DFT approach has been used to investigate the affinity of glycerol to adsorb on the CF and/or the deposited Ni. Material Studio® software was used, and all the geometries were optimized using forcite optimization in which the compass II was used in the force field, all the bulk atoms are fixed, and the surface of the Ni and graphite cleavage plans are (101 and 002), respectively, then Monto Carlo simulation was used to calculate the adsorption energy of glycerol.

3. Results and discussion

3.1. Material characterization

The effect of glycerol addition on the prepared catalyst morphology, composition, and structure is disclosed using

SEM. SEM images of CF, Ni@CF, $Ni_{0.05}$@CF, and $Ni_{0.5}$@CF are shown in Fig. 1(A–D). There is a significant agglomeration of the electrodeposited Ni onto CF in the Ni@CF as clearly seen in Fig. 1(B). The addition of 0.05 M glycerol into the deposition bath improves the particle distribution of the catalyst as can be seen in mapping EDX and at the same time reduces the average particle size of the catalyst from 290 nm to 220 nm, calculated using ImageJ® software. Consequently, a significant increase in the surface-active sites of the catalyst is expected, *c.f.* Fig. 3(A). This enhances the catalytic activity of the deposited Ni. This enhancement can be attributed to the adsorption of glycerol on the Ni catalyst during the electrodeposition step which is confirmed by the negative adsorption energy as revealed from the DFT calculation see Fig. 2(A). So, the rate of nucleation is increased, and the rate of growth is retarded. Obviously as shown in Fig. 1(D and D′), the deposited Ni sheets are detached from CF and cracked as the concentration of the glycerol is increased by more than 0.05 M. This is due to covering the CF surface with glycerol which acts as an insulating barrier causing the detaching of the deposited catalyst. Thus, the number of

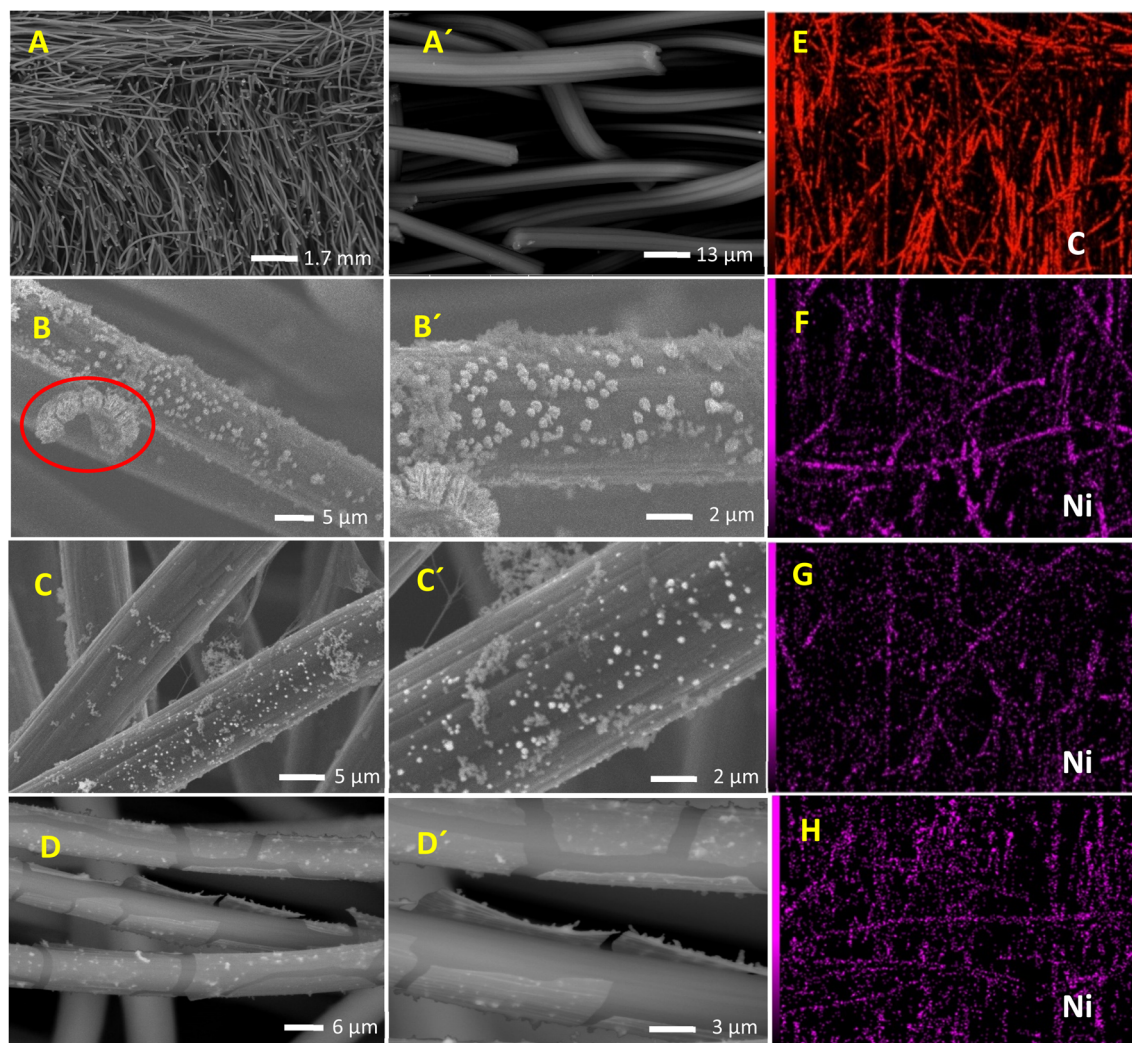**Fig. 1** SEM images for: (A and A′) CF, (B and B′) Ni@CF, (C and C′) $Ni_{0.05}$@CF, and (D and D′) $Ni_{0.5}$@CF electrodes at different magnifications. EDX color mapping of Ni for: (E) CF, (F) Ni@CF, (G) $Ni_{0.05}$@CF, and (H) $Ni_{0.5}$@CF electrodes.
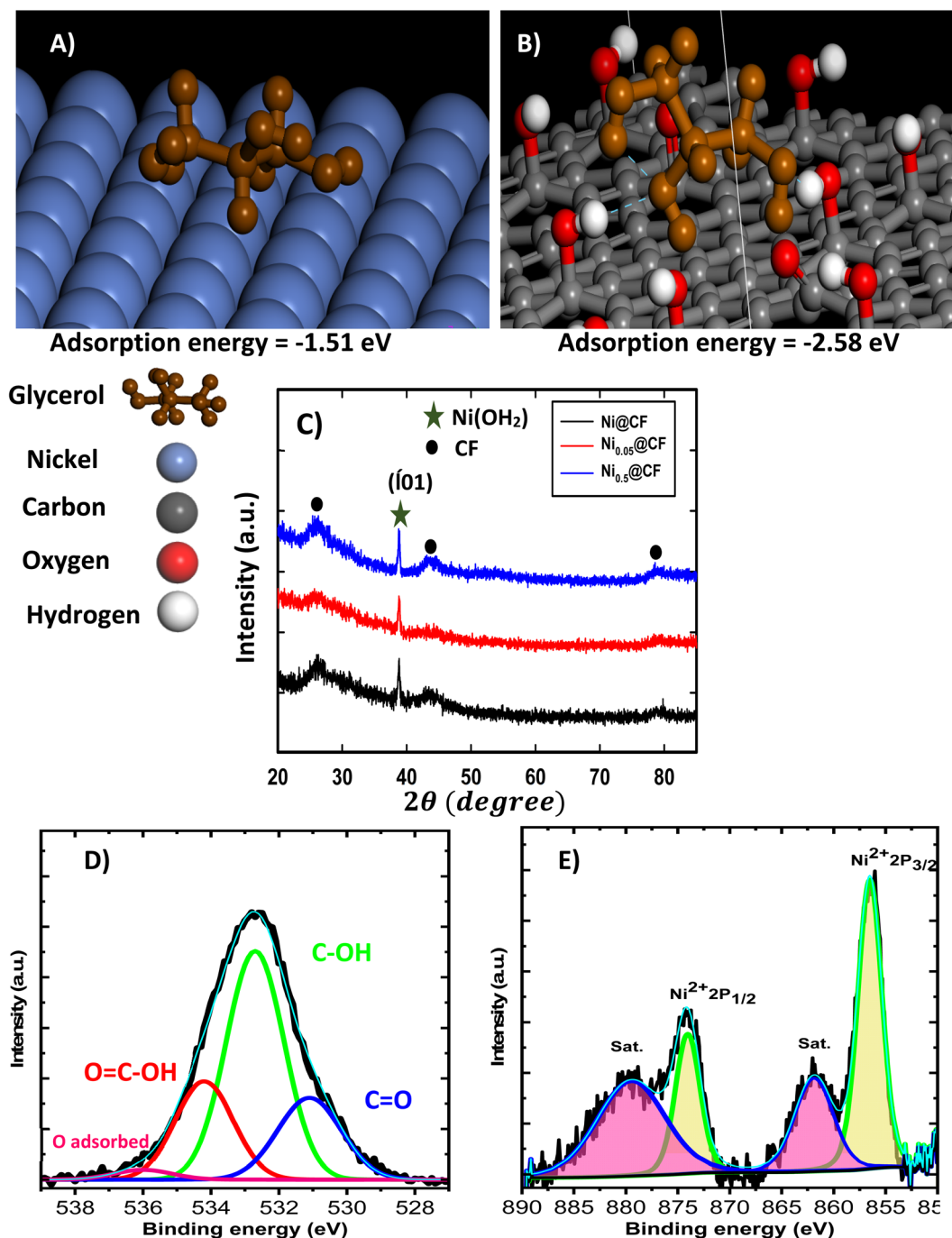
Fig. 2 Monto Carlo simulation for glycerol on Ni and CF surface (A) and (B), respectively. (C) XRD patterns of Ni@CF, $Ni_{0.05}$@CF, and $Ni_{0.5}$@CF electrodes. High resolution XPS spectrum of O 1s and Ni 2p for CF and $Ni_{0.05}$@CF electrode (D) and (E), respectively.

active sites available on the substrate is reduced and Ni layer starts to detach away from the CF and form sheets as can be seen in Fig. 1(D and D'). Additionally, from DFT calculations based on the geometers shown in Fig. 2(A and B), the adsorption energy calculated using Monto Carlo simulation of the glycerol onto the CF is markedly higher than its adsorption energy on Ni. Thus, at lower concentration of glycerol, there are remaining active sites onto the CF available for further electrodeposition and at the same time the adsorption of the glycerol occurs onto the electrodeposited Ni, while at higher concentrations of glycerol, CF surface becomes enriched in glycerol thus hinders the adherence of Ni.

XRD patterns of Ni@CF, $Ni_{0.05}$@CF and $Ni_{0.5}$@CF are displayed in Fig. 2(C) which are used to get information about their facets and crystallinity. As clearly seen, all the prepared electrodes show three diffraction peaks attributed to (002), (100), and (110) crystal planes of carbon which appear around 26°, 42°, and 77°, respectively, that agree with the (JCPDS ICDD card
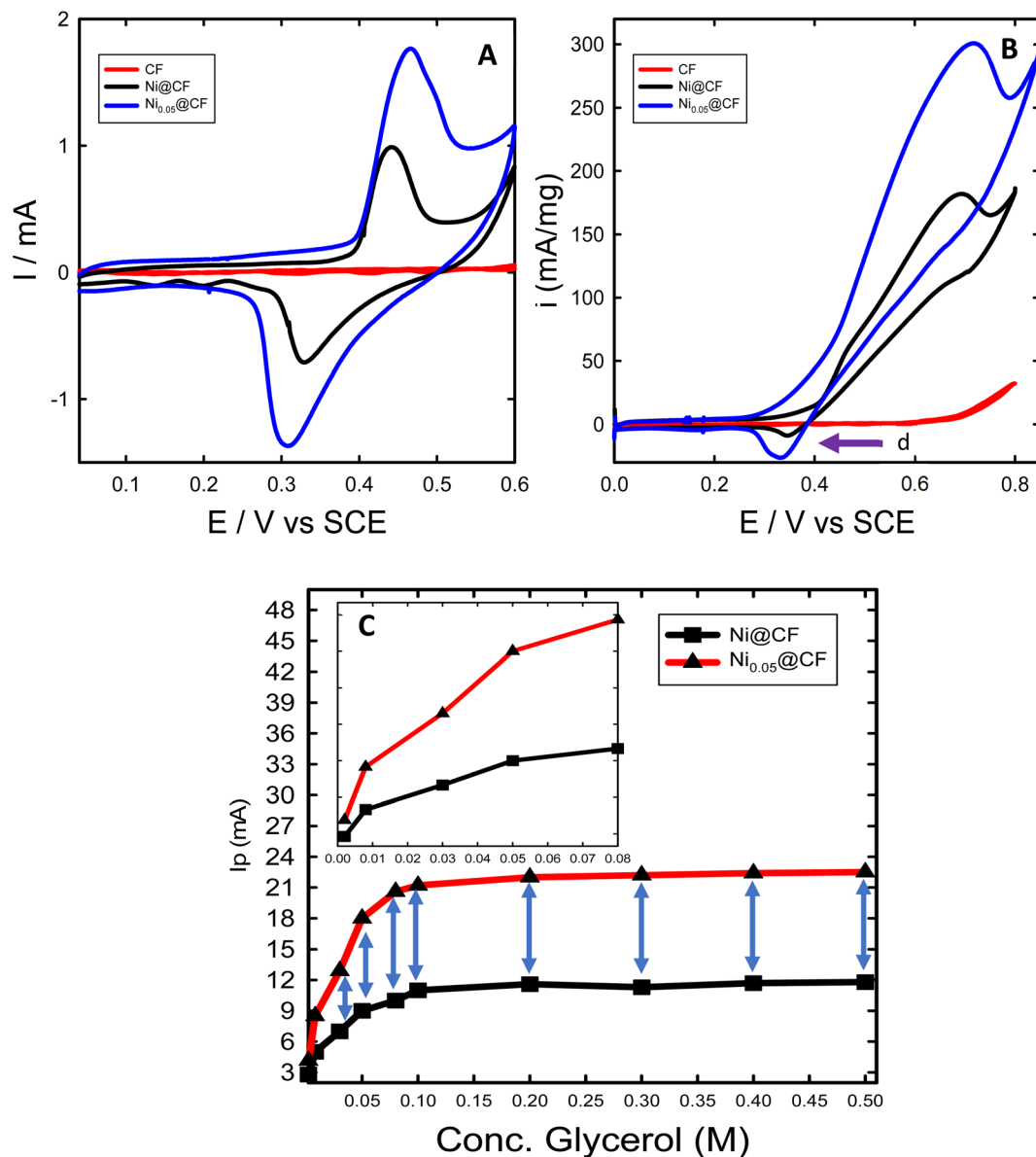
Fig. 3 CVs of CF (red line), Ni@CF (black line), and $Ni_{0.05}$@CF (blue line) measured in 0.1 M NaOH solution in absence (A) and in presence (B) of 8 mM glycerol with a same potential scan rate 10 mV s^{-1}. I_p of the glycerol electrooxidation for Ni@CF and $Ni_{0.05}$@CF as a function of glycerol concentration (0.002–0.5 M) (C) and inset of figure represent the zooming at the early stage of the two curves.

no. 00-001-0640). On the other hand, all the prepared electrodes show an additional peak at 38° attributed to the ($\bar{1}$01) crystal plane of Ni(OH)$_2$ that is consistant with the reference code (COD 1011134). To figure out the effect of addition of glycerol on the crystal size of electrodeposited Ni, Scherrer's equation is used to estimate the average crystal size for the prepared electrodes, as described in eqn (5)

$$D = \frac{0.9\lambda}{\beta \cos(\theta)} \quad (5)$$

where λ is the employed X-ray wavelength (1.54 Å), β is the peak's full width in radians at half maximum (FWHM), and θ is the peak's Bragg angle.[61,62] The addition of 0.05 M glycerol to the deposition bath led to a large decrease in the average crystal size

from 54 nm for Ni@CF to 36 nm for $Ni_{0.05}$@CF. However, increasing the concentration of glycerol > 0.05 M, the crystal size increases to *ca.* 42 nm for $Ni_{0.5}$@CF due to the excessive adsorption of glycerol on the CF that acts as an insulating barrier with raising the glycerol concentration as can be seen in Fig. 1(D and D′). The number of active sites on the CF available to the deposited of Ni reduced thus the rate of growth increased over than the rate of nucleation which agreed with the SEM and mapping EDX Fig. 1.

To figure out the surface state of the electrodeposited Ni, XPS analysis is performed, and the obtained O 1s and Ni 2p spectra are displayed in Fig. 2(D and E) for CF and $Ni_{0.05}$@CF. The O 1s is deconvoluted into four peaks to confirm the presence of the carbonyl, hydroxyl, and carboxylic functional groups into the CF
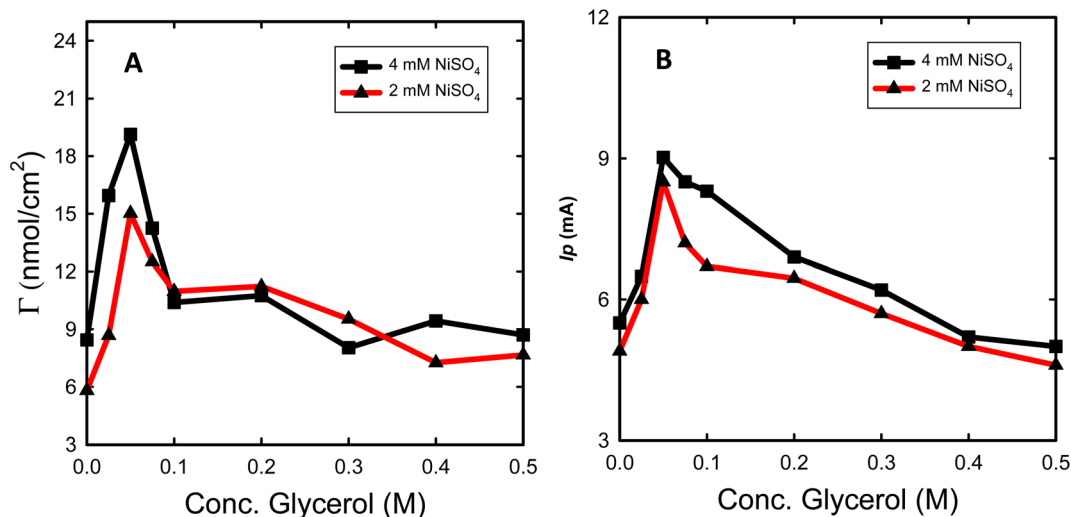
Fig. 4 Γ (A) and I_p (B) for the prepared Ni_x@CF electrode as a function of glycerol concentration for (2 (red line) and 4 (black line) mM) $NiSO_4$ with the same metal loading measured in 0.1 M NaOH without (A) and with (B) glycerol (8 mM) with a potential scan rate 10 mV s^{-1}.

to can be used in the DFT calculation. Moreover, the Ni 2p spectrum for $Ni_{0.05}$@CF typically shows Ni $2p_{3/2}$ and Ni $2p_{1/2}$ peaks with two satellites ("sat.") at binding energies 856.3 and 873.9 eV, respectively. The spin energy separation between them is found to be 17.6 eV which is characteristic of $Ni(OH)_2$.[63,64]

3.2. Glycerol electrooxidation

The performance of the prepared catalysts was investigated towards glycerol electrooxidation by using CV measurements. Fig. 3 shows the CVs of CF, Ni@CF, and $Ni_{0.05}$@CF electrodes in 0.1 M NaOH solution in the absence (Fig. 3(A)) and in the presence (Fig. 3(B)) of 8 mM glycerol. According to many articles,[15,34,41,60,65] the redox peak couple is observed at 0.45 V *vs.* SCE in Fig. 3(A) is attributed to NiOOH which is considered the active form toward glycerol electrooxidation where the larger the area under the peak, the more the activity obtained. As can be seen in Fig. 3(A) after adding 0.05 M glycerol in the deposition bath during the preparation of the catalyst, the NiOOH peak increases largely with the same metal loading and consequently, the activity of the catalyst is enhanced by about ≈1.6 times higher than Ni@CF and the onset potential is reduced by about 50 mV as can be concluded from Fig. 3(B). This is due to the adsorption of glycerol on the surface of the Ni catalyst during the electrodeposition on the CF which increases the rate of nucleation and retards the rate of growth. Therefore, better distribution and smaller particle size are obtained as shown in Fig. 1. Moreover, as notice peak (assigned by arrow d) in Fig. 3(B) represents the available sites from Ni catalyst and active for further glycerol electrooxidation which can be used if the concentration of the glycerol raised and can achieve enhancement higher than 1.6 times higher than Ni@CF thus, the electrooxidation of the glycerol for Ni@CF and $Ni_{0.05}$@CF was performed at higher concentration of glycerol as clearly seen in Fig. 3(C). A systematic increase in the I_p is obtained by raising the concentration of the glycerol until 0.1 M glycerol is

reached after that the steady state is obtained which means all of the active sites of Ni are participating in the electrooxidation. Moreover, the enhancement factor also increased by raising the concentration and reach 2 times higher than Ni@CF.

To figure out the enhancement of the oxidation current of the transformation of Ni to NiOOH as can be seen in Fig. 3(A) doesn't attributed to the traces of glycerol remaining on the electrode from the glycerol added in the deposition bath, the reduction peak of NiOOH to $Ni(OH)_2$ is also increased which means that the increase of current is due to better distribution of the catalyst' particles rather than the presence of glycerol. The surface concentration of the active phase is estimated from the amount of charge associated during the formation of the active phase using eqn (6):[45]

$$\Gamma = \frac{Q}{nFA} \qquad (6)$$

where, Γ is the surface concentration of the active phase (mol cm^{-2}), Q is the charge consumed during the formation of the active phase (Coulomb (C)), taking $n = 1$, F is Faraday's constant ($F = 96\,500$ C mol^{-1}) and A is the geometrical surface area of the substrate (0.52 cm^2). The estimated Γ increases from ~8 to ~19 nmol cm^{-2} for Ni@CF and $Ni_{0.05}$@CF, respectively. This means that the surface-active sites are increased 2.37 times by simple addition of 0.05 M glycerol to the deposition bath, which is adsorbed on the Ni catalyst during deposition, consequently better catalytic activity is obtained as can be seen in Fig. 3.

3.3. Optimization of glycerol concentration as additive

The effect of various glycerol concentrations added to the deposition bath was optimized for two deposition bath concentrations of $NiSO_4$ (2 and 4 mM). The same amount of Ni was electrodeposited to single out the effect of glycerol addition on the obtained electrocatalytic activity for glycerol oxidation. The estimated Γ and I_p (oxidation peak current for glycerol electrooxidation) for both concentrations of $NiSO_4$ for the
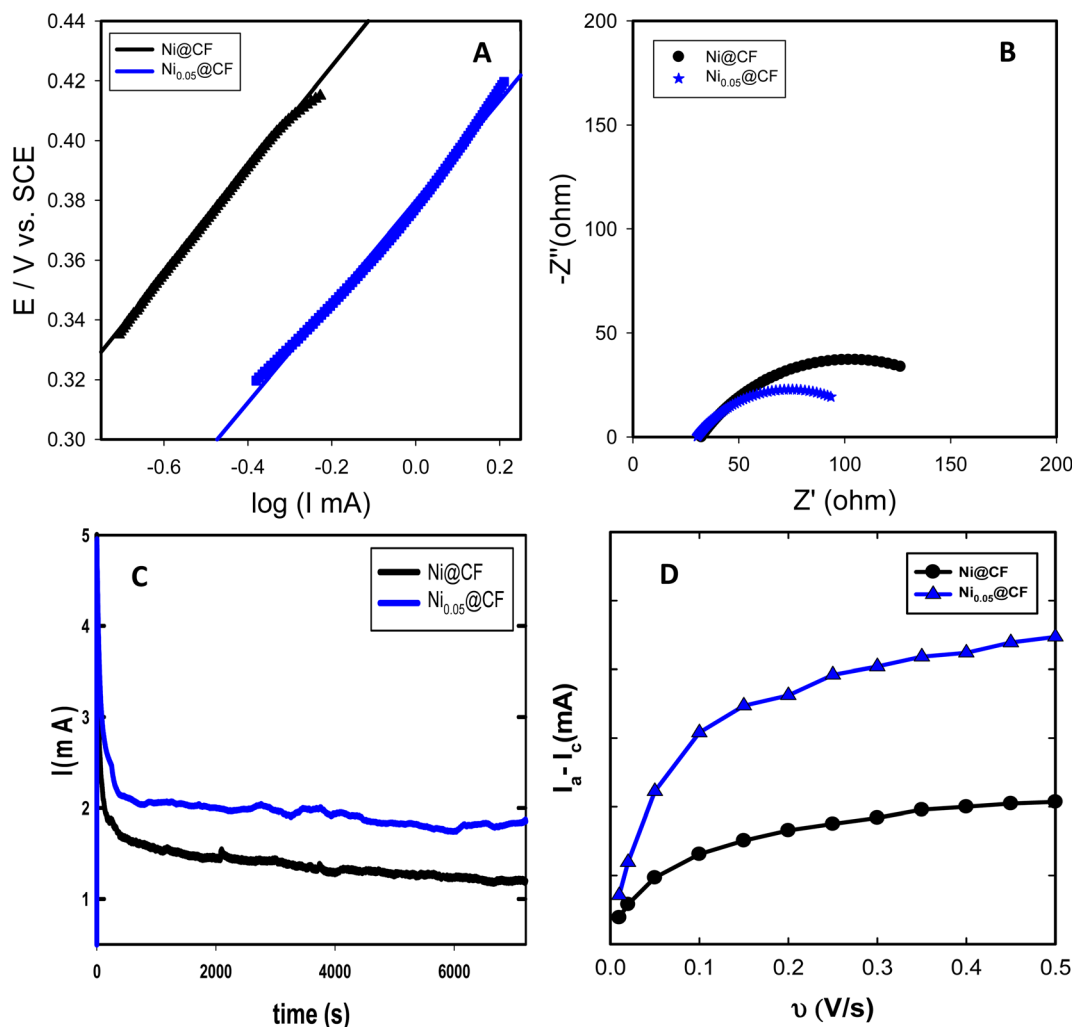
Fig. 5 (A) Tafel plots measured at potential scan rate 0.01 V s^{-1}. (B) Nyquist plots measured at 0.4 V. (C) Chronoamperometric curves measured at 0.6 V. All measurements are performed in 0.1 M NaOH solution containing 8 mM glycerol for Ni@CF and Ni$_{0.05}$@CF electrodes. (D) The estimation of electrochemical double layer capacitance (C_{dl}) for Ni@CF and Ni$_{0.05}$@CF by plotting ($I_c - I_a$) (capacitive current) *vs.* the potential scan rate in 0.1 M NaOH solution.

prepared Ni@CF and Ni$_x$@CF electrodes as a function of glycerol concentration are shown in Fig. 4. It is clearly seen in Fig. 4 that 0.05 M is the optimum glycerol concentration to be added to the deposition bath where it exhibits the highest I_p and Γ associated with the lowest onset potential for the glycerol electrooxidation. This can be attributed to the adsorption of glycerol on the electrodeposited Ni and the active sites of the CF increasing the rate of nucleation and decreasing the rate of growth with the reduction of the crystal size and hence improving the distribution of the catalyst as can be evidenced from SEM and XRD analysis. The more the glycerol concentration is increased, the more the reduction in I_p and Γ is obtained because of the excessive adsorption of glycerol on CF acts as an insulating barrier for Ni deposition. So, the number of active sites available on the CF is reduced. This leads to Ni sheets detached far away from the CF and at the same time crystal size increases as can be seen in Fig. 1(D and D′) and XRD data.

Raising the concentration of NiSO$_4$ from 2 to 4 mM also enhances I_p and Γ due to increasing the deposition efficiency.

3.3.1. Electrode kinetics. Tafel plots for the glycerol oxidation at Ni@CF and Ni$_{0.05}$@CF electrodes are investigated to reveal the effect of glycerol addition on the kinetics of electrooxidation as can be seen in Fig. 5(A). Tafel plots are measured in 0.1 M NaOH solution containing 8 mM glycerol at a potential scan rate of 10 mV s^{-1} and the electrodeposition is performed using a bath containing 4 mM NiSO$_4$. Tafel slopes of 173, and 168 mV dec^{-1} are calculated for Ni@CF and Ni$_{0.05}$@CF electrodes, respectively. The similarity in Tafel slopes indicates that the same rate-determining step dominates glycerol electrooxidation. Additionally, the exchange current (i_0) is estimated to be 69 and 111 μA for Ni@CF and Ni$_{0.05}$@CF electrodes, respectively. This supports the facile kinetics of the glycerol electrooxidation on Ni$_{0.05}$@CF as compared to Ni@CF electrode.

Table 1 A comparison of the electrocatalytic activity parameters of different Ni-based catalysts towards glycerol electrooxidation[a]

Catalyst	[NaOH] mol L^{-1}	[Glycerol] mol L^{-1}	Scan rate (mV s^{-1})	I (A g^{-1}) at 1.6 V $vs.$ RHE	Ref.
CoNi@C	0.1	0.1	50	0.063	41
FeCoNi@C	0.1	0.1	50	0.065	41
FeNi@C	0.1	0.1	50	0.052	41
NiCu@CCE	0.1	1.0	50	43.871	40
Ni@(CCE)	0.1	1.0	50	24.372	40
NiCo@CCE	0.1	1.0	50	116.990	40
Ni wire	1 M KOH	0.1	50	40.0	34
Ni doped porous Cu/Cu$_2$O	0.1	0.1	10	6.423	70
Ni@CF	0.2	0.008	10	126.0	This work
Ni$_{0.05}$@CF	0.2	0.008	10	**223.0**	

[a] CCE is carbon ceramic electrode.

Fig. 5(B) displays Nyquist plots of Ni@CF and Ni$_{0.05}$@CF electrodes measured in 0.1 M NaOH solution containing 8 mM glycerol at 0.4 V $vs.$ SCE and the electrodeposition of the catalyst performed using a deposition bath containing 4 mM NiSO$_4$. The electrooxidation of glycerol on Ni@CF and Ni$_{0.05}$@CF electrodes is found to be kinetically controlled due to the obtained semicircle illustration for Nyquist plots.[66,67] The experimentally measured Nyquist plots were fitted using Randle's equivalent circuit then calculating the charge transfer resistance (R_{ct}). The R_{ct} value is dropped from 140 ohm in the case of Ni@CF to 87 ohm using the Ni$_{0.05}$@CF electrode which shows that the Ni$_{0.05}$@CF electrode has a higher ability to oxidize glycerol which furtherly confirms that the addition of glycerol to the deposition bath enhances the catalytic activity of Ni catalyst towards glycerol electrooxidation.

The long-term stability of the prepared Ni@CF and Ni$_{0.05}$@CF electrodes is addressed via chronoamperometric (I–t) measurements at 0.6 V $vs.$ SCE for 2 h as displayed in Fig. 5(C). It is revealed from this data that the presence of 0.05 M glycerol in the deposition bath reduces the loss in the stability from 24 to 7% from their initial performance after only 750 s and at the same time increases the oxidation current by about 1.6 times after 2 h of continuous electrolysis as compared to Ni@CF electrode (in absence of glycerol in the Ni-deposition bath). Thus, Ni$_{0.05}$@CF electrode has better stability performance than Ni@CF electrode. Furthermore, our prepared catalysts show better electrocatalytic activity towards glycerol electrooxidation than previously published work, as compared in Table 1.

The reason behind the enhancement in the activity of the Ni$_{0.05}$@CF towards glycerol electrooxidation is the increment in the number of the active sites which comes from the better nucleation by the action of the additive. That reason can be also evidenced from the relation between the non-faradic capacitive current and scan rate for Ni@CF and Ni$_{0.05}$@CF to estimate the electrochemical surface area (ECSA) and the data are depicted in Fig. 5(D). As clearly seen in Fig. 5(D) the ECSA for Ni$_{0.05}$@CF is much higher than Ni@CF.[60,68] Moreover, the linear part obtained at low scan rates has a higher slope and consequently, indicating a larger fraction of the entire porous matrix is being contributing to the electrochemical surface area whereas at higher scan rates the top skin layer of the porous matrix contributes to the active area while the underlying porous matrix suffers from diffusion limitations.[69]

4. Conclusion

The presence of 0.05 M glycerol in the deposition bath of Ni electrodeposited on commercial CF resulted in boosting their performance towards glycerol electrooxidation. This enhancement was identified by about 2 times increase of the oxidation current as well as a $ca.$ 50 mV negative shift of its onset potential. This enhancement can be attributed to the adsorption of glycerol on the Ni catalyst during the electrodeposition step which is confirmed by the negative adsorption energy in DFT calculation thus, the rate of nucleation increases and the rate of growth decreases. The distribution of deposited Ni over the entire CF was improved concurrently with increasing their surface concentration and surface-active sites. The average crystal size of the electrodeposited Ni nanoparticles is reduced from 54 nm to 36 nm by the simple addition of 0.05 M glycerol to the deposition bath. Various glycerol concentrations (as additives) were optimized for the two different concentrations of Ni. The optimum deposition bath was composed of 4 mM NiSO$_4$ solution containing 0.05 M glycerol resulting in the electrocatalyst exhibiting the highest electrocatalytic activity for glycerol electrooxidation. The kinetics and stability of the Ni@CF towards glycerol electrooxidation are enhanced by adding 0.05 M glycerol, which is confirmed by EIS measurements, chronoamperometric curves, and Tafel plots. The charge transfer resistance is reduced from 140 to 87 ohm and loss in stability after 2 h of continuous electrolysis is also reduced from 24 to 7% by the simple addition of 0.05 M glycerol to the Ni deposition bath.

Conflicts of interest

There are no conflicts to declare.

References

1 E. Antolini and E. R. Gonzalez, $J. Power Sources$, 2010, **195**, 3431–3450.

2 A. H. Abu-ghazala, H. H. Abdelhady, A. A. Mazhar and M. S. El-Deab, *Renewable Energy*, 2022, **200**, 1120–1133.

3 B. C. Ong, S. K. Kamarudin and S. Basri, *Int. J. Hydrogen Energy*, 2017, **42**, 10142–10157.

4 H. Mou, Q. Chang, Z. Xie, S. Hwang, S. Kattel and J. G. Chen, *Appl. Catal., B*, 2022, **316**, 121648.

5 S. P. Viviane, N. Júlio, R. Andrezza and O. N. Almir, *J. Fuel Chem. Technol.*, 2022, **50**, 474–483.

6 M. R. Rizk, M. G. Abd El-Moghny, H. H. Abdelhady, W. M. Ragheb, A. H. Mohamed, H. F. Fouad, M. Mohsen, A. S. Kamel and M. S. El-Deab, *Int. J. Hydrogen Energy*, 2022, **47**, 32145–32157.

7 M. S. E. Houache, K. Hughes and E. A. Baranova, *Sustainable Energy Fuels*, 2019, **3**, 1892–1915.

8 A. Shukla, S. C. Singh, C. S. Saraj, G. Verma and C. Guo, *Mater. Today Chem.*, 2022, **23**, 100691.

9 A. L. Wang, H. Xu and G. R. Li, *ACS Energy Lett.*, 2016, **1**, 445–453.

10 S. Li, C. Xi, Y. Z. Jin, D. Wu, J. Q. Wang, T. Liu, H. B. Wang, C. K. Dong, H. Liu, S. A. Kulinich and X. W. Du, *ACS Energy Lett.*, 2019, **4**, 1823–1829.

11 Q. Zhang, C. Zhang, J. Liang, P. Yin and Y. Tian, *ACS Sustainable Chem. Eng.*, 2017, **5**, 3808–3818.

12 L. Chen, X. Dong, Y. Wang and Y. Xia, *Nat. Commun.*, 2016, **7**, 1–8.

13 D. Wang, Q. Li, C. Han, Z. Xing and X. Yang, *ACS Cent. Sci.*, 2018, **4**, 112–119.

14 S. Guan, X. Fu, Z. Lao, C. Jin and Z. Peng, *Sustainable Energy Fuels*, 2019, **3**, 2056–2066.

15 M. R. Rizk, M. G. Abd El-Moghny, A. Mazhar, M. S. El-Deab and B. E. El-Anadouli, *Sustainable Energy Fuels*, 2021, **5**, 986–994.

16 W. Ni, T. Wang, F. Héroguel, A. Krammer, S. Lee, L. Yao, A. Schüler, J. S. Luterbacher, Y. Yan and X. Hu, *Nat. Mater.*, 2022, **21**, 804–810.

17 L. Xie and D. W. Kirk, *J. Electrochem. Soc.*, 2020, **167**, 064519.

18 A. G. Oshchepkov, G. Braesch, A. Bonnefont, E. R. Savinova and M. Chatenet, *ACS Catal.*, 2020, **10**, 7043–7068.

19 R. M. Tesfaye, G. Das, B. J. Park, J. Kim and H. H. Yoon, *Sci. Rep.*, 2019, **9**, 1–9.

20 Y. Wang, Y. Wang, J. Zang, L. Dong, H. Pan and Y. Yuan, *Electrochim. Acta*, 2013, **113**, 583–590.

21 Z. Qi, H. Geng, X. Wang, C. Zhao, H. Ji, C. Zhang, J. Xu and Z. Zhang, *J. Power Sources*, 2011, **196**, 5823–5828.

22 S. Lee, H. J. Kim, S. M. Choi, M. H. Seo and W. B. Kim, *Appl. Catal., A*, 2012, **429–430**, 39–47.

23 M. Kapkowski, P. Bartczak, M. Korzec, R. Sitko, J. Szade, K. Balin, J. Lelątko and J. Polanski, *J. Catal.*, 2014, **319**, 110–118.

24 M. Simões, S. Baranton and C. Coutanceau, *Appl. Catal., B*, 2010, **93**, 354–362.

25 Y. Z. Su, Q. Z. Xu, Q. S. Zhong, C. J. Zhang, S. T. Shi and C. W. Xu, *Mater. Res. Bull.*, 2015, **64**, 301–305.

26 A. Y. Tsivadze, M. R. Tarasevich, V. A. Bogdanovskaya and M. R. Ehrenburg, *Dokl. Chem.*, 2008, **419**, 54–56.

27 E. Lohrasbi and M. Asgari, *Adv. Anal. Chem.*, 2015, **5**, 9–18.

28 M. A. Goda, M. G. Abd El-Moghny and M. S. El-Deab, *J. Electrochem. Soc.*, 2020, **167**, 064522.

29 A. M. Ahmed, S. Y. Sayed, G. A. El-Nagar, W. M. Morsi, M. S. El-Deab and B. E. El-Anadouli, *J. Electroanal. Chem.*, 2019, **835**, 313–323.

30 Y. Zhao, L. Fan, J. Ren and B. Hong, *Int. J. Hydrogen Energy*, 2014, **39**, 4544–4557.

31 A. Papaderakis, N. Pliatsikas, C. Prochaska, K. M. Papazisi, S. P. Balomenou, D. Tsiplakides, P. Patsalas and S. Sotiropoulos, *Front. Chem.*, 2014, **2**, 1–11.

32 D. Soundararajan, J. H. Park, K. H. Kim and J. M. Ko, *Curr. Appl. Phys.*, 2012, **12**, 854–859.

33 Y. Hong, H. J. Kim, H. J. Lee, J. Kim and S. Il Choi, *Front. Chem.*, 2019, **7**, 1–9.

34 M. S. E. Houache, E. Cossar, S. Ntais and E. A. Baranova, *J. Power Sources*, 2018, **375**, 310–319.

35 M. Rizk, M. Abd El-Moghny and M. El-Deab, *J. Electrochem. Soc.*, 2020, **167**, 114505.

36 Y. Kang, W. Wang, Y. Pu, J. Li, D. Chai and Z. Lei, *Chem. Eng. J.*, 2017, **308**, 419–427.

37 R. M. A. Tehrani and S. Ab Ghani, *Electrochim. Acta*, 2012, **70**, 153–157.

38 D. P. M. Fleischmann and K. Korinek, *J. Chem. Soc., Perkin trans. II*, 1971, 1312–1315.

39 V. L. Oliveira, C. Morais, K. Servat, T. W. Napporn, G. Tremiliosi-Filho and K. B. Kokoh, *J. Electroanal. Chem.*, 2013, **703**, 56–62.

40 B. Habibi and N. Delnavaz, *RSC Adv.*, 2016, **6**, 31797–31806.

41 V. L. Oliveira, C. Morais, K. Servat, T. W. Napporn, G. Tremiliosi-Filho and K. B. Kokoh, *Electrochim. Acta*, 2014, **117**, 255–262.

42 M. S. E. Houache, K. Hughes, R. Safari, G. A. Botton and E. A. Baranova, *ACS Appl. Mater. Interfaces*, 2020, **12**, 15095–15107.

43 B. Habibi and N. Delnavaz, *RSC Adv.*, 2016, **6**, 31797–31806.

44 G. A. El-Nagar, I. Derr, T. Kottakkat and C. Roth, *ECS Trans.*, 2017, **80**, 1013–1022.

45 M. E. Ghaith, G. A. El-Nagar, M. G. Abd El-Moghny, H. H. Alalawy, M. E. El-Shakre and M. S. El-Deab, *Int. J. Hydrogen Energy*, 2020, **45**, 9658–9668.

46 M. D. de Jesus Almeida, C. A. Della Rovere, L. R. P. de AndradeLima, D. V. Ribeiro and C. A. C. De Souza, *Mater. Res.*, 2019, **22**(4), e20180480.

47 M. Mouanga, L. Ricq, J. Douglade and P. Berçot, *J. Appl. Electrochem.*, 2007, **37**, 283–289.

48 H. Nakano, T. Ura, S. Oue and S. Kobayashi, *ISIJ Int.*, 2014, **54**, 1653–1660.

49 K. Krishnadevi, S. RatnaKumari, D. Prasanna, H. B. N. Prasanna and V. Anuradha, *J. Colloid Interface Sci.*, 2022, **607**, 1776–1785.

50 B. Jaleh, M. Nasrollahzadeh, M. Eslamipanah, A. Nasri, E. Shabanlou, N. R. Manwar, R. Zboril, P. Fornasiero and M. B. Gawande, *Carbon*, 2022, **198**, 301–352.

51 R. Zeng, K. Lian, B. Su, L. Lu, J. Lin, D. Tang, S. Lin and X. Wang, *Angew. Chem., Int. Ed.*, 2021, **60**, 25055–25062.

52 F. C. Lee, M. S. Ismail, D. B. Ingham, K. J. Hughes, L. Ma, S. M. Lyth and M. Pourkashanian, *Renewable Sustainable Energy Rev.*, 2022, **166**, 112640.

53 T. X. H. Le, M. Bechelany and M. Cretin, *Carbon*, 2017, **122**, 564–591.

54 R. E. G. Smith, T. J. Davies, N. D. B. Baynes and R. J. Nichols, *J. Electroanal. Chem.*, 2015, **747**, 29–38.

55 A. Di Blasi, O. Di Blasi, N. Briguglio, A. S. Aricò, D. Sebastián, M. J. Lázaro, G. Monforte and V. Antonucci, *J. Power Sources*, 2013, **227**, 15–23.

56 Y. Wang and Y. Hasebe, *Talanta*, 2009, **79**, 1135–1141.

57 L. Han, S. Tricard, J. Fang, J. Zhao and W. Shen, *Biosens. Bioelectron.*, 2013, **43**, 120–124.

58 Z. González, A. Sánchez, C. Blanco, M. Granda, R. Menéndez and R. Santamaría, *Electrochem. Commun.*, 2011, **13**, 1379–1382.

59 K. J. Kim, Y. J. Kim, J. H. Kim and M. S. Park, *Mater. Chem. Phys.*, 2011, **131**, 547–553.

60 M. E. Ghaith, M. G. A. El-moghny, G. A. El-nagar, H. H. Alalawy, M. E. El-Shakre and M. S. El-Deab, *RSC Adv.*, 2023, **13**, 895–905.

61 N. Benipal, J. Qi, J. C. Gentile and W. Li, *Renewable Energy*, 2017, **105**, 647–655.

62 I. H. Karahan, H. A. Çetinkara and H. S. Güder, *Int. J. Surf. Eng. Coatings*, 2013, **86**, 157–161.

63 H. Jiang, Y. Guo, T. Wang, P. L. Zhu, S. Yu, Y. Yu, X. Z. Fu, R. Sun and C. P. Wong, *RSC Adv.*, 2015, **5**(17), 12931–12936.

64 J. Yan, Z. Fan, W. Sun, G. Ning, T. Wei, Q. Zhang, R. Zhang, L. Zhi and F. Wei, *Adv. Funct. Mater.*, 2012, **22**, 2632–2641.

65 A. M. Abdelrahim, M. G. Abd El-Moghny, M. E. El-Shakre and M. S. El-Deab, *RSC Adv.*, 2023, **13**, 1811–1822.

66 M. A. Goda, M. G. Abd El-Moghny and M. S. El-Deab, *J. Electrochem. Soc.*, 2020, **167**, 064522.

67 I.-M. Hsing, X. Wang and Y.-J. Leng, *J. Electrochem. Soc.*, 2002, **149**, A615.

68 I. O. Baibars, M. G. Abd El-Moghny and M. S. El-Deab, *J. Environ. Chem. Eng.*, 2022, **10**, 2.

69 C. Costentin and J. M. Savéant, *ACS Appl. Energy Mater.*, 2019, **2**, 4981–4986.

70 M. R. Rizk, M. G. Abd El-Moghny, G. A. El-Nagar, A. A. Mazhar and M. S. El-Deab, *ChemElectroChem*, 2020, **7**, 951–958.